I&EC research
Industrial & Engineering Chemistry Research

Article

pubs.acs.org/IECR

# On Heuristic Computation and Application of Flexibility Indices for Unsteady Process Design

Yi-Chung Kuo and Chuei-Tin Chang*

Department of Chemical Engineering, National Cheng Kung University, Tainan 70101, Taiwan

**ABSTRACT:** The unsteady chemical processes, designed according to the nominal operating conditions and fixed model parameters, have traditionally been evaluated with economic criteria. This design strategy often ends up with a plant which may become inoperable if some of the process conditions/parameters unexpectedly deviate from their normal levels. Two alternative performance measures, the dynamic and temporal flexibility indices, have thus been devised in recent years to characterize designs from a different viewpoint. However, not only their significances still have not been adequately interpreted and their roles clarified, but also their numerical values cannot be determined efficiently with the available algorithms. In this study, the simple trapezoidal rule is applied to discretize and integrate the dynamic models and a heuristic strategy is then utilized to implement the vertex method for computing the aforementioned metrics efficiently. To demonstrate the effectiveness of the proposed computation approaches, comprehensive case studies concerning two dynamic systems, that is, the buffer system and the solar-driven membrane distillation desalination system (SMDDS), have been carried out. The resulting insights have also been summarized in a heuristic design procedure to incorporate both indices for general applications.

## 1. INTRODUCTION

Dealing with uncertainties is one of the practical issues in designing and operating chemical plants. These so-called uncertainties are not always stochastic, as they may arise either from the unexpected exogenous disturbances (such as those in feed qualities, product demands, and environmental conditions, etc.) or from the uncharacterizable estimation errors of model parameters (such as heat transfer coefficients, reaction rate constants, and other physical properties).[1−4] The ability of a chemical process to maintain feasible operation despite uncertain deviations from the nominal states is often referred to as its *operational flexibility*,[5,6] which is clearly an issue of key importance that must be addressed in any design. Various approaches to facilitate quantitative flexibility analysis have already been proposed in numerous studies.[1−16]

The original *steady-state flexibility index* ($FI_s$) was defined by Swaney and Grossmann[5,6] for use as a gauge of the feasible region in the parameter space. Specifically, this index is associated with the maximum allowable deviations of the uncertain parameters from their nominal values, by which feasible operation can be assured with proper manipulation of the control variables. These authors also showed that, under certain convexity assumptions, critical points that limit flexibility must be on the vertices of the uncertain parameter space. Grossmann and Floudas[9] later exploited the fact that the active constraints represent bottlenecks of a design and developed a mixed integer nonlinear programming (MINLP) model accordingly. Similar analyses have also been carried out in a series of subsequent studies to address various issues in producing resilient and operable designs.[17−19] Since the steady-state material-and-energy balances are used as the equality constraints in the aforementioned model, $FI_s$ can be viewed as a performance indicator of the *continuous* process under consideration.

On the other hand, Dimitriadis and Pistikopoulos[20] noted that the operational flexibility of a dynamic (or batch) system must be evaluated differently. Specifically, the *dynamic flexibility index* ($FI_d$) should be computed by adopting a system of differential algebraic equations (DAEs) as the model constraints. Dimitriadis et al.[21] studied the operational feasibility issue for the purpose of safety verification, while Zhou et al.[22] utilized a similar approach to assess the operational flexibility of batch systems. Notice also that, in order to calculate this $FI_d$, the nominal values of uncertain parameters and the anticipated positive and negative deviations in these parameters are assumed to be available at every instance over the entire time horizon of operation life. The index value can be uniquely determined on the basis of a dynamic system model and also such *a priori* information. However, while an ill designed system may become inoperable due to disturbances in some process parameters at certain instances, the cumulative effects of temporary variations in finite time intervals can also result in serious consequences. Although the latter scenario is ignored in the conventional dynamic flexibility analysis, it is sometime a more probable event in practical applications. To address this important issue, a mathematical programming model has been developed by Adi and Chang[23] for evaluating the corresponding performance measure, which was referred to as the *temporal flexibility index* ($FI_t$). They also successfully applied this new performance measure in the designs of the solar-driven membrane distillation desalination system[24] and the hybrid power generation systems.[25]

From the above discussions, one can see that the dynamic and temporal flexibility indices may complement one another to fully characterize a given unsteady process and, thus, it should be advantageous to consider *both* in a design. However, the computation and application strategies of these indices still have not been developed well enough for design purposes. Not

**Received:** September 25, 2015
**Revised:** December 18, 2015
**Accepted:** January 5, 2016
**Published:** January 5, 2016

ACS Publications © 2016 American Chemical Society



DOI: 10.1021/acs.iecr.5b03593
*Ind. Eng. Chem. Res.* 2016, 55, 670−682

only their significances have not been accurately interpreted and their roles not clarified, but also their numerical values cannot be computed effectively with the existing algorithms originally developed for their steady-state counterparts. Clearly further studies are needed to address these implementation issues, and the present work represents a first attempt to tackle these challenging problems. In particular, a shortcut computation strategy has been adopted to simplify the exhaustive enumeration procedure of the traditional vertex method,[8] and this strategy is facilitated with simple heuristics that can be used to limit the search scope to only a small portion of all possible vertexes. Furthermore, a heuristic design procedure has also been developed to incorporate both indices for a wide variety of design applications.

The rest of the paper is organized as follows. The general formulation for modeling the unsteady processes is first given in the next section, which also includes two alternative constraints for characterizing uncertainties. The dynamic and temporal flexibility indices are defined accordingly with different mathematical programming models in section 3, while in the next section two improved versions of the conventional vertex method are presented for solving these models, respectively. To provide clear illustration of the proposed formulations and the required solution steps, simple examples concerning the continuous and periodic buffer operations are presented in section 5. An additional more realistic example, that is, the solar driven membrane distillation desalination system (SMDDS), is presented in section 6 to demonstrate the applicability and usefulness of the proposed models. Finally, in section 7, conclusions are drawn and a heuristic design procedure is also devised according to the insights gained from case studies.

## 2. DESIGN MODEL OF UNSTEADY PROCESSES

For illustration clarity, let us first introduce two label sets to enumerate and classify all constraints in a given model:

$$\mathbb{I} = \{i | i \text{ is the label of an equality constraint in the design model}\} \tag{1}$$

$$\mathbb{J} = \{j | j \text{ is the label of an inequality constraint in the design model}\} \tag{2}$$

The $i$th equality constraint in this design model can be expressed in a general form as

$$h_i(\mathbf{d}, \mathbf{z}(t), \mathbf{x}(t), \dot{x}(t), \boldsymbol{\theta}(t)) = 0 \tag{3}$$

where $i \in \mathbb{I}$, $t \in [0, H]$, and $\mathbf{x}(0) = \mathbf{x}^0$; $\mathbf{d}$ represents a constant vector in which all design specifications are stored; $\mathbf{z}(t)$ denotes the time-variant vector of all adjustable control variables; $\mathbf{x}(t)$ is the time-variant vector of all state variables; $\boldsymbol{\theta}$ denotes the time-variant vector of all uncertain parameters. Notice that $h_i$ is essentially a *functional* of various functions of time and the corresponding constraint is usually established to model the dynamic behavior of a given unsteady process (e.g., the transient mass or energy balance equation of a reactor). Similarly, the $j$th inequality constraint in this model can be written as

$$g_j(\mathbf{d}, \mathbf{z}(t), \mathbf{x}(t), \boldsymbol{\theta}(t)) \le 0 \tag{4}$$

where $j \in \mathbb{J}$ and $g_j$ is also a functional. Note that eq 4 is often adopted to reflect the actual physical and/or chemical boundaries in the given process (e.g., a capacity limit).

The time-dependent upper and lower bounds of the aforementioned uncertain parameters are also incorporated in the present model, that is,

$$\boldsymbol{\theta}^N(t) - \Delta\boldsymbol{\theta}^-(t) \le \boldsymbol{\theta}(t) \le \boldsymbol{\theta}^N(t) + \Delta\boldsymbol{\theta}^+(t) \tag{5}$$

These bounds are formulated with *given* time functions, that is, $\boldsymbol{\theta}^N(t)$, $\Delta\boldsymbol{\theta}^-(t)$, and $\Delta\boldsymbol{\theta}^+(t)$, which may be extracted directly from historical records of observable parameters. For example, by setting $H$ to be 24 h, these time functions may be established according to the largest range of *hourly* rainfall data collected every day over a period of several months.

On the other hand, if the cumulated quantities of such parameters over time are also recorded, the following extra inequalities may be adopted to fully characterize the uncertain parameters

$$-\Delta\boldsymbol{\Theta}^- \le \boldsymbol{\Theta}(H) \le +\Delta\boldsymbol{\Theta}^+ \tag{6}$$

where

$$\boldsymbol{\Theta}(t) = \int_0^t [\boldsymbol{\theta}(\tau) - \boldsymbol{\theta}^N(\tau)]\, \mathrm{d}\tau \tag{7}$$

For the purpose of illustration, let us consider the previous example again. The scalar values of $\Delta\boldsymbol{\Theta}^-$ and $\Delta\boldsymbol{\Theta}^+$ in this scenario can now be estimated according to the *daily* rainfall data which are usually also available. Since it is often the case that the uncertain parameters do not always stay at the upper (or lower) limits throughout the entire horizon $[0,H]$, one would expect

$$\Delta\boldsymbol{\Theta}^- \le \int_0^H \Delta\boldsymbol{\theta}^-(\tau)\, \mathrm{d}\tau \tag{8}$$

$$\Delta\boldsymbol{\Theta}^+ \le \int_0^H \Delta\boldsymbol{\theta}^+(\tau)\, \mathrm{d}\tau \tag{9}$$

## 3. DYNAMIC AND TEMPORAL FLEXIBILITY INDICES

According to Dimitriadis and Pistikopoulos,[20] the *dynamic flexibility index* $\mathrm{FI_d}$ can be computed on the basis of the following model:

$$\mathrm{FI_d} = \max \delta_\mathrm{d} \tag{10}$$

subject to eq 3 and

$$\max_{\boldsymbol{\theta}(t)} \min_{\mathbf{z}(t),\mathbf{x}(t)} \max_{j,t} g_j(\mathbf{d}, \mathbf{z}(t), \mathbf{x}(t), \boldsymbol{\theta}(t)) \le 0 \tag{11}$$

$$\boldsymbol{\theta}^N(t) - \delta_\mathrm{d}\Delta\boldsymbol{\theta}^-(t) \le \boldsymbol{\theta}(t) \le \boldsymbol{\theta}^N(t) + \delta_\mathrm{d}\Delta\boldsymbol{\theta}^+(t) \tag{12}$$

Note that the scalar variable $\delta_\mathrm{d}$ is used here to adjust the range of $\boldsymbol{\theta}(t)$ in eq 12 and this practice is essentially the direct extension of its steady-state counterpart.

Since there are obvious incentives to develop a quantitative flexibility measure that takes in account of the accumulated effects of uncertain parameters in nonsteady operations, Adi and Chang[23] proposed to use the following model for computing a so-called *temporal flexibility index* $\mathrm{FI_t}$:

$$\mathrm{FI_t} = \max \delta_\mathrm{t} \tag{13}$$

subject to eq 3, 5, 11, and

$$-\delta_\mathrm{t}\Delta\boldsymbol{\Theta}^- \le \boldsymbol{\Theta}(H) \le +\delta_\mathrm{t}\Delta\boldsymbol{\Theta}^+ \tag{14}$$

Note that the scalar variable $\delta_\mathrm{t}$ is used here to adjust the range of the accumulated quantities in eq 14, while the transient variations of uncertain parameters are bound between the *original* upper and lower limits, that is, eq 3. On the other hand, in computing the dynamic flexibility index $\mathrm{FI_d}$ described previously, the former constraints are in fact not used whereas the latter are modified with $\delta_\mathrm{d}$ instead. In particular applications, the proper parameter



DOI: 10.1021/acs.iecr.5b03593
Ind. Eng. Chem. Res. 2016, 55, 670−682

constraints can be selected on a case-by-case basis by considering the availability of historical data and the intrinsic nature of uncertainties.

## 4. EXTENDED VERTEX METHODS

Although basically other alternative numerical strategies (such as the extended versions of active set method) may be developed as well, the extended vertex methods have been adopted in the present study to compute the dynamic and temporal flexibility indices. While an accurate estimate of the flexibility index cannot be guaranteed theoretically for a given nonconvex system,[5,6] the critical points may still be located at the vertexes in most cases even when the required convexity conditions are not met.[26] Furthermore, to relieve the heavy computation load caused by the overwhelmingly large number of vertexes, effective selection heuristics are also adopted in this work to limit the search scope to only a small number of candidates. This approach is especially attractive in practical applications due to its implementation easiness.

The proposed methods are briefly summarized below:

**4.1. Discretization of Dynamic Model.** An indispensable preparation step for computing the aforementioned indices is to discretize the DAEs in eq 3 on the basis of a credible numerical technique. Although many candidates are available, only the simple trapezoidal rule is presented in the sequel to facilitate clear understanding. For the purpose of illustration, let us rewrite the differential equations in eq 3 in an alternative formulation as follows

$$\frac{\mathrm{d}\mathbf{x}(t)}{\mathrm{d}t} = \boldsymbol{\varphi}(\mathbf{d}, \mathbf{x}(t), \mathbf{z}(t), \boldsymbol{\theta}(t)) \tag{15}$$

or

$$\frac{\mathrm{d}x_i(t)}{\mathrm{d}t} = \varphi_i(\mathbf{d}, \mathbf{x}(t), \mathbf{z}(t), \boldsymbol{\theta}(t)), \quad i \in \mathbb{I} \tag{16}$$

Note that every algebraic equation in the same model can also be expressed in this form by setting $\dot{x}_i(t) = 0$. Let us then divide the horizon $[0,H]$ into $M$ equal intervals and label their boundary points sequentially as $p = 0, 1, 2, \cdots, M$. Thus, the length of each interval should be

$$h = \frac{H}{M} \tag{17}$$

By applying the trapezoidal rule to estimate the integral of $\varphi_i(\mathbf{d}, \mathbf{x}(t), \mathbf{z}(t), \boldsymbol{\theta}(t))$ over each interval, one could obtain

$$x_i(t_p) = x_i(t_{p-1}) + \frac{h}{2}[\varphi_i(\mathbf{d}, \mathbf{x}(t_{p-1}), \mathbf{z}(t_{p-1}), \boldsymbol{\theta}(t_{p-1})) + \varphi_i(\mathbf{d}, \mathbf{x}(t_p), \mathbf{z}(t_p), \boldsymbol{\theta}(t_p))] \tag{18}$$

where $x_i(0) = x_i^0, i \in \mathbb{I}$ and $p = 1, 2, \cdots, M$. Similarly, eq 4 can also be discretized according to the aforementioned boundary points as follows

$$g_j(\mathbf{d}, \mathbf{x}(t_p), \mathbf{z}(t_p), \boldsymbol{\theta}(t_p)) \le 0 \quad \forall\, j \in \mathbb{J} \tag{19}$$

**4.2. Computation of Dynamic Flexibility Index.** The dynamic version of the original vertex method[8] can be formulated as a two-level optimization problem, that is,

$$\mathrm{FI_d} = \min_{k} \max_{\mathbf{z}(t),\mathbf{x}(t)} \delta_\mathrm{d} \tag{20}$$

subject to eqs 3 and 4, and also the following constraint in a function space formed by all possible time profiles of $\boldsymbol{\theta}(t)$:

$$\boldsymbol{\theta}(t) = \boldsymbol{\theta}^k(t) = \boldsymbol{\theta}^N(t) + \delta_\mathrm{d}\Delta\boldsymbol{\theta}^k(t) \tag{21}$$

where $\Delta\boldsymbol{\theta}^k(t)$ denotes a vector pointing from the nominal point $\boldsymbol{\theta}^N(t)$ toward the $k$th vertex ($k = 1, 2, 3, \cdots, 2^{N_\mathrm{p}}$ and $N_\mathrm{p}$ is the number of uncertain parameters) at time $t$. Note that each element in $\Delta\boldsymbol{\theta}^k(t)$ should be obtained from the corresponding entry in either $-\Delta\boldsymbol{\theta}^-(t)$ or $\Delta\boldsymbol{\theta}^+(t)$.

For illustration clarity, let us next produce a specific formulation by discretizing the above model with the trapezoidal rule:

$$\mathrm{FI_d} = \min_{k} \max_{\mathbf{z},\mathbf{x}} \delta_\mathrm{d} \tag{22}$$

subject to eqs 17−19 and

$$\boldsymbol{\theta}(t_p) = \boldsymbol{\theta}^N(t_\mathrm{p}) + \delta_\mathrm{d}\Delta\boldsymbol{\theta}^k(t_p), \quad p = 1, 2, ..., M \tag{23}$$

where $\mathbf{X} = [\mathbf{x}(t_1)\ \mathbf{x}(t_2)\ \cdots\ \mathbf{x}(t_M)]$ and $\mathbf{Z} = [\mathbf{z}(t_1)\ \mathbf{z}(t_2)\ \cdots\ \mathbf{z}(t_M)]$.

**4.3. Computation of Temporal Flexibility Index.** The vertex locations of a hypercube defined by eq 14 can be expressed mathematically as

$$\boldsymbol{\Theta}(H) = \delta_\mathrm{t}\Delta\boldsymbol{\Theta}^k \tag{24}$$

where $\Delta\boldsymbol{\Theta}^k$ denotes a vector pointing from the origin (i.e., the nominal point) in the $N_p$-dimensional Euclidean space toward the $k$th vertex and each element in $\Delta\boldsymbol{\Theta}^k$ must be the same as the corresponding entry in either $-\Delta\boldsymbol{\Theta}^-$ or $\Delta\boldsymbol{\Theta}^+$. From the definition of $\boldsymbol{\Theta}(H)$ $(= \int_0^H[\boldsymbol{\theta}(\tau) - \boldsymbol{\theta}^N(\tau)]\,\mathrm{d}\tau)$, it is clear that every vertex can be reached with an infinite number of time profiles that are bounded according to eq 5. Therefore, to be able to implement the temporal version of the vertex method in realistic applications, it is obviously necessary to reduce the search space to a manageable size.

It has been found in the study that, in addition to eq 5, a useful heuristic can be adopted to further constrain the candidate time profiles of uncertain parameters for use in eq 24, that is,

$$\Delta\hat{\theta}_n^k(t;\, t_0^n,\, t_\mathrm{f}^n) = \hat{\theta}_n^k(t;\, t_0^n,\, t_\mathrm{f}^n) - \theta_n^N(t) = \begin{cases} \Delta\theta_n^k(t), & \text{if } 0 < t_0^n \le t \le t_\mathrm{f}^n < H \\ 0, & \text{if } 0 \le t < t_0^n \text{ or } t_\mathrm{f}^n < t \le H \end{cases} \tag{25}$$

where, $n = 1, 2, \cdots, N_\mathrm{p}$; $k = 1, 2, 3, \cdots, 2^{N_\mathrm{p}}$; $\theta_n^N(t)$ is the $n$th vector element of $\boldsymbol{\theta}^N(t)$ defined in eq 5; $\Delta\theta_n^k(t)$ represents the $n$th element of a vector pointing from the nominal point $\boldsymbol{\theta}^N(t)$ toward the $k$th vertex of the hypercube defined by eq 5. More specifically, the position of this vertex can be expressed as

$$\boldsymbol{\theta}(t) = \hat{\boldsymbol{\theta}}^k(t) = \boldsymbol{\theta}^N(t) + \Delta\hat{\theta}^k(t) \tag{26}$$

where

$$\hat{\boldsymbol{\theta}}^k(t) = [\hat{\theta}_1^k(t;\, t_0^1,\, t_\mathrm{f}^1)\ \ \hat{\theta}_2^k(t;\, t_0^2,\, t_\mathrm{f}^2)\ \ \cdots\ \ \hat{\theta}_{N_p}^k(t;\, t_0^{N_p},\, t_\mathrm{f}^{N_p})]^\mathrm{T}$$

$$\boldsymbol{\theta}^N(t) = [\theta_1^N(t)\ \ \theta_2^N(t)\ \ \cdots\ \ \theta_{N_p}^N(t)]^\mathrm{T}$$

$$\Delta\hat{\boldsymbol{\theta}}^k(t) = [\Delta\hat{\theta}_1^k(t;\, t_0^1,\, t_\mathrm{f}^1)\ \ \Delta\hat{\theta}_2^k(t;\, t_0^2,\, t_\mathrm{f}^2)\ \ \cdots\ \ \Delta\hat{\theta}_{N_p}^k(t;\, t_0^{N_p},\, t_\mathrm{f}^{N_p})]^\mathrm{T}$$

As mentioned previously, $\Delta\hat{\boldsymbol{\theta}}^k(t)$ can be treated as a vector in the *functional space* of $\boldsymbol{\theta}(t)$ which starts from the nominal point $\boldsymbol{\theta}^N(t)$ and ends at the $k$th vertex and, in addition, each element of



DOI: 10.1021/acs.iecr.5b03593
Ind. Eng. Chem. Res. 2016, 55, 670−682

$\Delta\hat{\boldsymbol{\theta}}^k(t)$ should be selected from the corresponding entry in either $-\Delta\boldsymbol{\theta}^-(t)$ or $\Delta\boldsymbol{\theta}^+(t)$. Notice also that, as clearly indicated in eq 25, the allowed deviation in each uncertain parameter may begin and terminate at instances which are not the same as those of the other parameters. Finally, although the justification for the aforementioned heuristics is derived from an intuitive belief, that is, the most serious disturbance a realistic process can withstand is usually the one with the largest possible magnitude, its validity has been verified by numerically simulating the worse-case scenarios in extensive case studies and, also, by solving the same problems independently with the active set method. The latter will be reported in a future paper.

In principle, $FI_t$ can be determined by solving eqs 3, 11, 13, and 24−26 via discretization and, for illustration simplicity, let us again utilize the trapezoidal rule for this purpose in the sequel. Since the starting and ending times of parameter deviations, i.e., $t_0^n$, $t_f^n$ and $n = 1, 2, \cdots, N_p$, are not given a priori, an extra binary variable $\varepsilon_p^n \in \{0,1\}$ must be introduced at every discretized time $t_p^n$ to reflect if the corresponding maximum deviation, i.e., $\Delta\theta_n^k(t_p^n)$, takes place. Thus, after dropping the parameters $t_0^n$ and $t_f^n$, eq 25 can be discretized and rewritten as

$$\hat{\theta}_n^k(t_p^n) - \theta_n^N(t_p^n) = \begin{cases} \Delta\theta_n^k(t_p^n) & \text{if } \varepsilon_p^n = 1 \\ 0 & \text{if } \varepsilon_p^n = 0 \end{cases} \tag{27}$$

With these binary variables, additional logic constraints can be incorporated in a mathematical programming model to enforce the heuristic in eq 25. Specifically, if the aforementioned disturbance in $\theta_n$ starts at a particular discretized time $t_{p'}^n$, then eqs 25 and 26 can be expressed as follows

$$\varepsilon_{p'}^n = 1 \tag{28}$$

$$\varepsilon_0^n = \varepsilon_1^n = \ldots = \varepsilon_{p'-1}^n = 0 \tag{29}$$

$$(1 - \varepsilon_p^n) + \varepsilon_{p+1}^n \le 1 \tag{30}$$

where $p' \in \{1, 2, \ldots, M-1\}$ and $p = p', p'+1, \cdots, M-1$. Equation 30 clearly implies that

1. If deviation is not present at $t_p^n$ (i.e., $\varepsilon_p^n = 0$), then there will not be any at the next instance $t_{p+1}^n$ (i.e., $\varepsilon_{p+1}^n = 0$);
2. If otherwise (i.e., $\varepsilon_p^n = 1$), then the disturbance at $t_{p+1}^n$ may or may not take place (i.e., $\varepsilon_{p+1}^n = 0$ or 1).

Consequently, eq 26 can be rewritten as

$$\theta_n(t_p^n) = \theta_n^N(t_p^n) + \varepsilon_p^n \Delta\theta_n^k(t_p^n) \tag{31}$$

where $p = 1, 2, \cdots, M$, $n = 1, 2, \cdots, N_p$, and $k = 1, 2, 3, \cdots, 2^{N_p}$. Then the accumulated quantity of parameter variation can then be expressed accordingly as

$$\Theta_n(H) = \sum_{p=1}^{M} \varepsilon_p^n \Delta\theta_n^k(t_p^n) \tag{32}$$

where $n = 1, 2, \cdots, N_p$, and $k = 1, 2, 3, \cdots, 2^{N_p}$. Finally, the discretized version of eq 14 should be

$$-\delta_t \Delta\Theta_n^- \le \sum_{p=1}^{M} \varepsilon_p^n \Delta\theta_n^k(t_p^n) \le \delta_t \Delta\Theta_n^+ \tag{33}$$

where $n = 1, 2, \cdots, N_p$ and $k = 1, 2, 3, \cdots, 2^{N_p}$.

By making use of the above formulations, a MINLP model can be constructed to realize the temporal version of vertex method; that is,

$$FI_t = \min_{k,\varepsilon} \max_{\mathbf{Z},\mathbf{X},\mathbf{E}} \delta_t \tag{34}$$

subject to eqs 17−19 and 28−33. More specifically,

$$\mathbf{E} = \begin{bmatrix} \varepsilon_1^1 & \varepsilon_2^1 & \cdots & \varepsilon_M^1 \\ \varepsilon_1^2 & \varepsilon_2^2 & \cdots & \varepsilon_M^2 \\ \vdots & \vdots & \cdots & \vdots \\ \varepsilon_1^{N_p} & \varepsilon_2^{N_p} & \cdots & \varepsilon_M^{N_p} \end{bmatrix}$$

$$\mathbf{X} = [\mathbf{x}(t_1) \quad \mathbf{x}(t_2) \quad \cdots \quad \mathbf{x}(t_M)]$$

$$\mathbf{Z} = [\mathbf{z}(t_1) \quad \mathbf{z}(t_2) \quad \cdots \quad \mathbf{z}(t_M)]$$

$$\boldsymbol{\varepsilon} = [\varepsilon_{p_1'}^1 \quad \varepsilon_{p_2'}^2 \quad \cdots \quad \varepsilon_{p_{N_p}'}^{N_p}]^T$$

$$p_1', p_2', \cdots, p_{N_p}' \in \{1, 2, \cdots, M-1\}$$

$$k \in \{1, 2, 3, \cdots, 2^{N_p}\}$$

## 5. ILLUSTRATIVE EXAMPLES

Let us consider the buffer tank in Figure 1. The dynamic model of this system can be written as

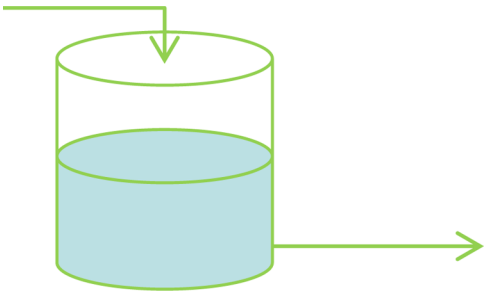

**Figure 1.** A buffer vessel.

$$A \frac{dh}{dt} = \theta(t) - k\sqrt{h} \tag{35}$$

where $h$ denotes the height of liquid level (m); $A$ (= 5 $m^2$) is the cross-sectional area of the tank; $k$ ($=\sqrt{5}/10$ $m^{5/2}$ $min^{-1}$) is a proportionality constant; $\theta$ denotes the feed flow rate ($m^3$ $min^{-1}$) and it is treated as the only uncertain parameter in the present example. To fix ideas, the following upper and lower limits are also adopted in the flexibility analysis: (i) The height of tank is 10 m; that is, $h \le 10$. (ii) Because of the operational requirement of downstream unit(s), the outlet flow rate of the buffer tank must be kept above $\sqrt{5}/10$ $m^3$ $min^{-1}$. Thus, the minimum allowable height of its liquid level should be 1 m; that is, $1 \le h$. (iii) The time horizon covers a period of 800 min; that is, $0 \le t \le 800$.

To facilitate interpreting the dynamic and temporal flexibility indices, two different operation modes are considered in the sequel: continuous and periodic.

**5.1. Example 1: Continuous Operation.** Let us assume that, in the continuous operation under consideration, the nominal steady-state value of feed rate is $\theta^N(t) = 0.5$ $m^3$ $min^{-1}$



DOI: 10.1021/acs.iecr.5b03593
Ind. Eng. Chem. Res. 2016, 55, 670−682

and the anticipated positive and negative deviations are set at $\Delta\theta^{+}(t) = \Delta\theta^{-}(t) = 0.5\ m^3\ min^{-1}$. Therefore, the range of uncertain parameter is

$$0 \le \theta(t) \le 1 \tag{36}$$

and the nominal height of liquid level at steady state should be 5 m. By discretizing eq 35 according to the trapezoidal rule (see subsection 4.1) and then applying the dynamic version of the extended vertex method (see subsection 4.2), one can evaluate the corresponding dynamic flexibility index, and its value is 0.415.

The above result indicates that, while the present operation is infeasible, $FI_d$ can be raised to the operational target of 1 if the expected range of uncertain parameter can be narrowed to

$$0.5 - 0.415 \times 0.5 \le \theta(t) \le 0.5 + 0.415 \times 0.5 \tag{37}$$

by improving the flow control quality of the feed stream. This assertion can be verified by carrying out numerical simulations of the worst-case scenarios (see Figure 2). One can observe that, if

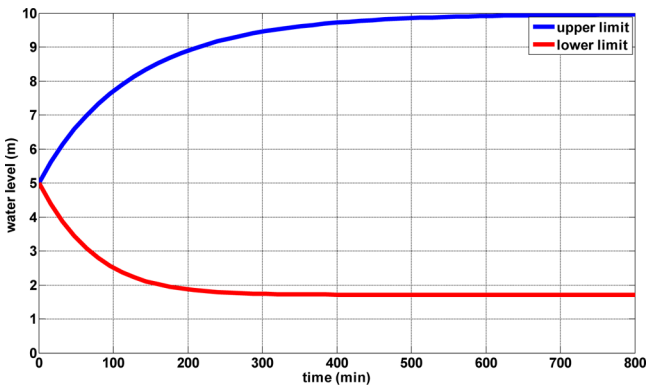


**Figure 2.** Simulation results of the worst-case scenarios for the narrowed parameter range defined in eq 37 in Example 1.

the feed rate is maintained respectively at the upper and lower limits of the narrowed range defined in eq 37, the water level can be guaranteed to satisfy the operational constraints at any time throughout the given horizon. In addition, two other observations should also be noted: (i) the water level approaches 10 m (i.e., the upper bound of $h$) at 800 min in the former scenario; (ii) the water level always stays considerably above the lower limit (i.e., $h > 1$) in the latter case

Note finally that, if it is not possible to improve the control quality of the upstream feed stream, the operational target of $FI_d = 1$ can be realized alternatively by increasing the buffer capacity. In particular, a larger storage tank with a cross-sectional area of 61 $m^2$ can be adopted to replace the original one to withstand all possible disturbances allowed by eq 36.

To facilitate computation of temporal flexibility index in the present example, let us further set the accumulated positive and negative deviations in liquid volumes ($m^3$) to be

$$\Delta\Theta^{+} = \Delta\Theta^{-} = 62.5 \tag{38}$$

In other words, the feed rate in the anticipated worse-case scenario is required to be reduced to the lower limit (i.e., 0.0 $m^3\ min^{-1}$) or raised to the upper bound (1.0 $m^3\ min^{-1}$) for a period of 125 (= 62.5/0.5) minutes. By solving the proposed model, it can be found that $FI_t = 0.444$ and this implies that the given system can only withstand the most severe disturbance for 55.5 (= 125 × 0.444) minutes. Figure 3 shows the simulation results of two corresponding scenarios. One can observe that the

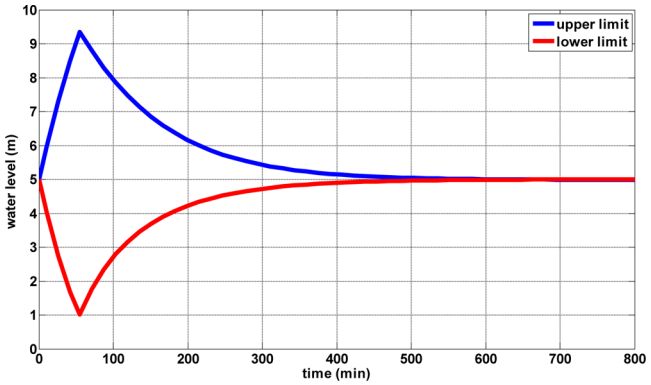


**Figure 3.** Simulation results of the worst-case scenarios in Example 1 ($FI_t = 0.444$, $A = 5\ m^2$, $t_0 = 0$ min, $t_f = 55.5$ min).

water level (i) just touches 1 m (i.e., the lower bound of $h$) at 55.5 min after introducing the largest negative disturbance at 0 min; (ii) always stays considerably below the upper limit (i.e., $h < 10$) if the largest positive disturbance lasts only 55.5 min.

The former is obviously the worst case. Note that the same lower bound of eq 14 can also be reached by lowering the feed rate slightly to 0.4653 $m^3\ min^{-1}$ (= 0.5 − (62.5 × 0.444)/800) throughout the entire horizon, but the corresponding water level should always remain in the feasible range according to eq 37.

As mentioned previously, the value of $FI_d$ can be improved to 1 by increasing the cross-sectional area of the buffer vessel from 5 $m^2$ to 61 $m^2$. Since a relatively large tank is called for, the required investment may not be justifiable. However, if it can be predicted on the basis of operation experience that the largest disturbances rarely last for the entire horizon, then the less stringent design criterion of $FI_t = 1$ may be acceptable. The corresponding area for this goal should be 11.3 $m^2$ and the required capital cost is obviously much lower. Figure 4 shows the simulation results of the worst-case scenarios for $FI_t = 1$ in Example 1.

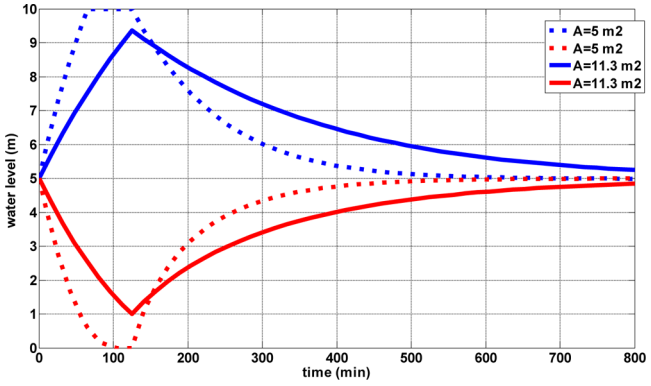


**Figure 4.** Simulation results of the worst-case scenarios in Example 1. ($FI_t = 1$, $A = 5$ or 11.3 $m^2$, $t_0 = 0$ min, $t_f = 55.5$ min).

**5.2. Example 2: Periodic Operation.** Let us next assume that, over a single period of 800 min in the cyclic operation under consideration, the nominal feed rate and its anticipated positive and negative deviations can be described below in eq 39 and also in Figure 5. The initial height of liquid level in this example is also set at 5 m.



DOI: 10.1021/acs.iecr.5b03593
Ind. Eng. Chem. Res. 2016, 55, 670−682

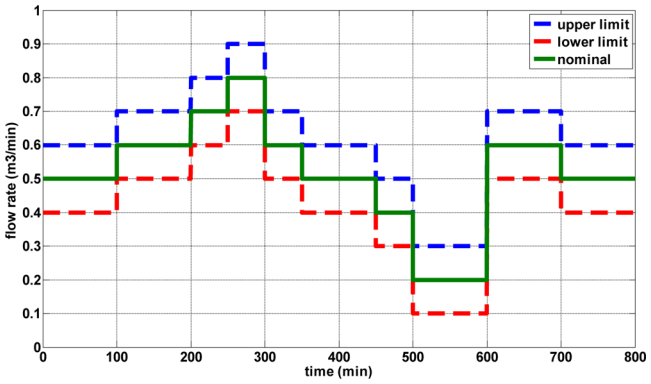


**Figure 5.** Nominal feed rate and its upper and lower limits in a single period in Example 2.

$$\begin{cases} \theta^N(t) = 0.5(\mathrm{m}^3\ \mathrm{min}^{-1}),\ \Delta\theta^+(t) = \Delta\theta^-(t) = 0.1 \\ \quad \text{for } 0 \le t \le 100(\mathrm{min}) \\ \theta^N(t) = 0.6(\mathrm{m}^3\ \mathrm{min}^{-1}),\ \Delta\theta^+(t) = \Delta\theta^-(t) = 0.1 \\ \quad \text{for } 100 \le t \le 200(\mathrm{min}) \\ \theta^N(t) = 0.7(\mathrm{m}^3\ \mathrm{min}^{-1}),\ \Delta\theta^+(t) = \Delta\theta^-(t) = 0.1 \\ \quad \text{for } 200 \le t \le 250(\mathrm{min}) \\ \theta^N(t) = 0.8(\mathrm{m}^3\ \mathrm{min}^{-1}),\ \Delta\theta^+(t) = \Delta\theta^-(t) = 0.1 \\ \quad \text{for } 250 \le t \le 300(\mathrm{min}) \\ \theta^N(t) = 0.6(\mathrm{m}^3\ \mathrm{min}^{-1}),\ \Delta\theta^+(t) = \Delta\theta^-(t) = 0.1 \\ \quad \text{for } 300 \le t \le 350(\mathrm{min}) \\ \theta^N(t) = 0.5(\mathrm{m}^3\ \mathrm{min}^{-1}),\ \Delta\theta^+(t) = \Delta\theta^-(t) = 0.1 \\ \quad \text{for } 350 \le t \le 450(\mathrm{min}) \\ \theta^N(t) = 0.4(\mathrm{m}^3\ \mathrm{min}^{-1}),\ \Delta\theta^+(t) = \Delta\theta^-(t) = 0.1 \\ \quad \text{for } 450 \le t \le 500(\mathrm{min}) \\ \theta^N(t) = 0.2(\mathrm{m}^3\ \mathrm{min}^{-1}),\ \Delta\theta^+(t) = \Delta\theta^-(t) = 0.1 \\ \quad \text{for } 500 \le t \le 600(\mathrm{min}) \\ \theta^N(t) = 0.6(\mathrm{m}^3\ \mathrm{min}^{-1}),\ \Delta\theta^+(t) = \Delta\theta^-(t) = 0.1 \\ \quad \text{for } 600 \le t \le 700(\mathrm{min}) \\ \theta^N(t) = 0.5(\mathrm{m}^3\ \mathrm{min}^{-1}),\ \Delta\theta^+(t) = \Delta\theta^-(t) = 0.1 \\ \quad \text{for } 700 \le t \le 800(\mathrm{min}) \end{cases} \tag{39}$$

By discretizing eq 35 according to the trapezoidal rule and then applying the dynamic vertex method, one can find that the corresponding dynamic flexibility index is 0.368. This index value indicates that, although the present operation is infeasible, $FI_d$ can be made to achieve 1 by reducing the range of variation in the uncertain parameter; that is,

$$\theta^N(t) - 0.368 \times \Delta\theta^-(t) \le \theta(t) \le \theta^N(t) + 0.368 \times \Delta\theta^+(t) \tag{40}$$

where $\theta^N(t)$, $\Delta\theta^-(t)$ and $\Delta\theta^+(t)$ are defined in eq 39. Figure 6 shows the simulation results of the corresponding worst-case scenarios. Note that, if the feed rate is maintained respectively at the upper and lower limits of the narrowed parameter range defined in eq 40, the water level should stay within the allowed range; that is, $1 \le h \le 10$, at any time throughout the given horizon, and also, it can be observed that the water level reaches (i) 10 m (which is the upper bound of $h$) at 300 min in the former scenario and (ii) 1 m (which is the lower bound of $h$) at 600 min in the latter scenario.

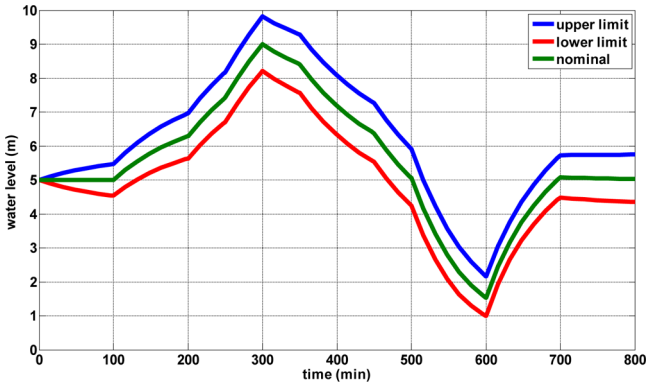


**Figure 6.** Simulation results of the worst-case scenarios for the narrowed parameter range defined in eq 40 in Example 2.

Finally, note that the operational target of $FI_d = 1$ can also be achieved by enlarging the cross-sectional area of the buffer tank to 8.25 $m^2$. The simulation results of the corresponding worse-case scenarios can be found in Figure 7.

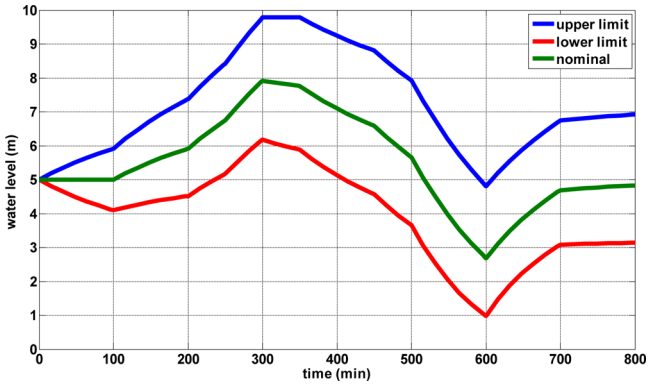


**Figure 7.** Simulation results of the worst-case scenarios for the original parameter range defined in eq 39 and an enlarged buffer tank in Example 2.

To facilitate concrete computation of temporal flexibility index in the present case, let us assign the accumulated positive and negative deviations in liquid volumes ($m^3$) to be

$$\Delta\Theta^+ = \Delta\Theta^- = 20.0 \tag{41}$$

By discretizing eq 35 according to the trapezoidal rule and then implementing the temporal vertex method, one can find that the corresponding temporal flexibility index is 0.185 for which the disturbance exists in the time interval between 562 and 599 min. These results imply that, when the largest deviation in feed rate is present in the above period, an accumulated volume decrease of 3.7 ($= 20 \times 0.185$) $m^3$ should cause the water level reaching the lower limit of 1 m at the end point of this time interval. This prediction can be clearly observed in the simulation results presented in Figure 8. Finally, notice that the temporal flexibility in this case can also be enhanced with a larger tank. From the optimum solution of the proposed programming model, one can deduce that at least a cross-sectional area of 6.95 $m^2$ should be adopted to achieve the designated design target; that is, $FI_t = 1$. The corresponding simulation results can be found in Figure 9.

## 6. ADDITIONAL CASE STUDIES

Additional flexibility analyses on various configurations of the SMDDS have also been performed in this work to further



DOI: 10.1021/acs.iecr.5b03593
Ind. Eng. Chem. Res. 2016, 55, 670−682

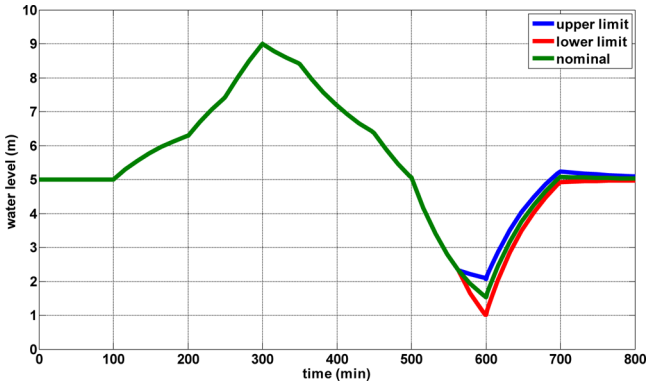


**Figure 8.** Simulation results of the worst-case scenarios in Example 2 ($FI_t$ = 0.185, $A$ = 5 m$^2$, $t_0$ = 562 min, $t_f$ = 599 min).

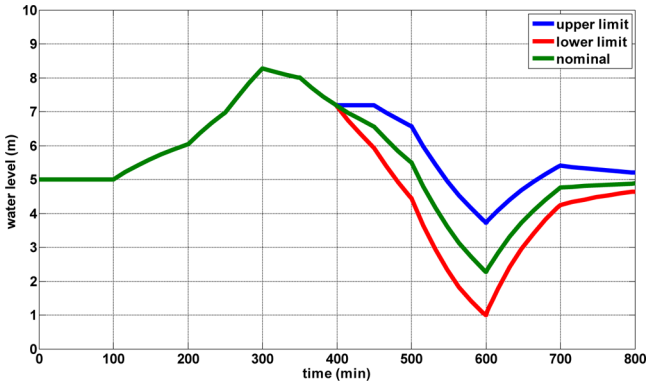


**Figure 9.** Simulation results of the worst-case scenarios in Example 2 ($FI_t$ = 1, $A$ = 6.95 m$^2$, $t_0$ = 399 min, $t_f$ = 599 min).

validate the proposed computation and design strategies. It should be noted first that Ben Bacha et al.[27] and Chang et al.[28,29] have already built mathematical models of all SMDDS units, that is, (1) the solar absorber, (2) the thermal storage tank, (3) the counter-flow shell-and-tube heat exchanger, (4) the AGMD modules, and (5) the distillate tank. Obviously a realistic system design must be fully functional in the presence of uncertain sunlight radiation and unpredictable freshwater demand. To achieve a desired flexibility target, the aforementioned units must be sized properly and also the corresponding thermal storage scheme must be synthesized in a rational fashion. If the solar absorber is relatively small when compared with the membrane distillation unit, then it may be beneficial to operate the stripped-down SMDDS shown in Figure 10 (Structure 1). Otherwise, at least one thermal storage tank must be adopted to buffer the drastic energy surplus incurred during daytime operation. Structure 2 in Figure 11 is the simplest design for such a purpose, while more elaborate configurations can certainly be devised to further enhance operational flexibility. For examples, two smaller thermal storage tanks may be placed in series according to Figure 12 (Structure 3) or in parallel according to Figure 13 (Structure 4). For the sake of completeness, the mathematical models of all units embedded in the above structures are presented in Appendix I and all model parameters and variables used in our case studies are also listed in Appendix II.

The solar irradiation rate $I(t)$ should obviously be treated as a time-variant uncertain parameter in the flexibility analyses. Its nominal profile $I^N(t)$, which is similar to that suggested by Chang et al.,[28] and its expected upper and lower bounds are depicted in

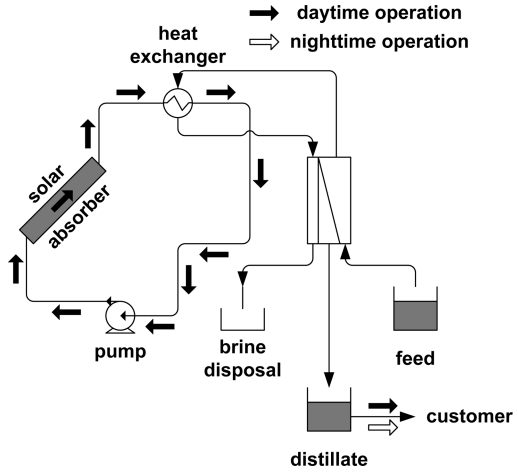


**Figure 10.** Structure 1 of SMDDS system.

Figure 14. Note that the expected positive and negative deviations at any time are both set at 10% of the nominal level. The largest accumulated positive and negative deviations of $I(t)$ are both assumed to be 2 × 10$^6$ J/m$^2$.

The water demand rate $m_{DT_{out}}(t)$ is the second uncertain parameter considered in the case studies. Its nominal value is set at 18 kg/h × wdf($t$), where wdf($t$) is the ratio between the demand rate at time $t$ and a reference value (i.e., 18 kg/h). The expected deviations in $m_{DT_{out}}$ are also selected to be 10% of its nominal value. The nominal level of wdf($t$) and also the corresponding upper and lower limits are sketched in Figure 15. Finally, the maximum accumulated positive and negative deviations of water demand are both set to be 40 kg.

In all cases, the specifications of a standard AGMD module are assumed to be the same as those given in Banat et al.,[30] and its effective membrane area is 10 m$^2$. On the basis of eqs A8−A10, the production rate of each AGMD module at $T^{HX}_{CL_{out}}$ = 74 °C is estimated to be 16.54 kg/h (assuming that the feed temperature is $T^{HX}_{CL_{in}}$ = 25 °C). The nominal mass flow rate of seawater in membrane distillation loop $m^N_{MD}$ is set to be 1125 kg/h per AGMD module according to Banat et al.[30] Also, a maximum daily demand of 750.42 kg/day can be computed according to Figure 15. By adopting an average online period of 12 h/day, the approximate number of parallel AGMD modules can be calculated:

$$n_{AGMD} = \frac{750.42}{16.54 \times 12} = 3.78 \approx 4 \quad (42)$$

Thus, the total membrane area used in the case studies should be 40 m$^2$.

In the solar absorber, the total mass of operating fluid per unit area, i.e., $M_{SA}/A_{SA}$, is set to be 15 kg/m$^2$.[28] The flow rate in the solar thermal loop ($m_{STL}$) is chosen to be 36000 kg/h, which is 8 times the total nominal flow rate of seawater in the membrane distillation loop ($m^N_{MD}$ = 1125 × 4 = 4500 kg/h). This value is selected to ensure quick temperature response in the desalination loop. The volume of distillate tank in each structure is assumed to be 0.75 m$^3$ ($A_{DT}$ = 0.35 m$^2$; $h_{DT,low}$ = 0 m; $h_{DT,high}$ = 2.14 m). A 10 m$^3$ thermal storage tank ($M_{ST}$ = 10000 kg) is adopted in structure 2, while each tank in structures 3 and 4 is exactly half this capacity. Finally, it is assumed that the heat capacity of operating fluid $C_p$ is held constant at 4200 J/(kg °C), and its density $\rho$ is also assumed to be constant at 1000 kg/m$^3$.



DOI: 10.1021/acs.iecr.5b03593
Ind. Eng. Chem. Res. 2016, 55, 670−682

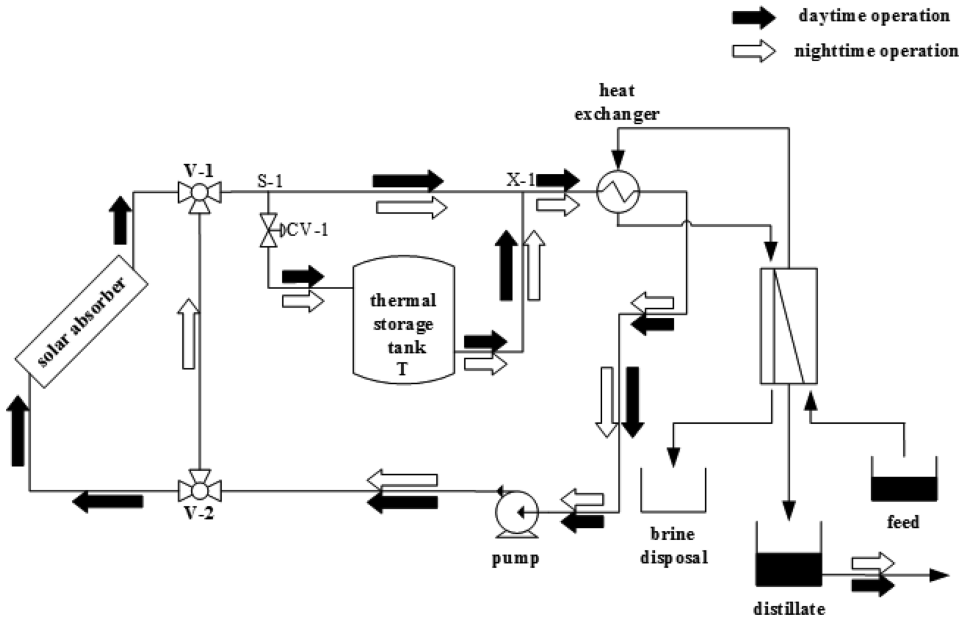


**Figure 11.** Structure 2 of SMDDS system.

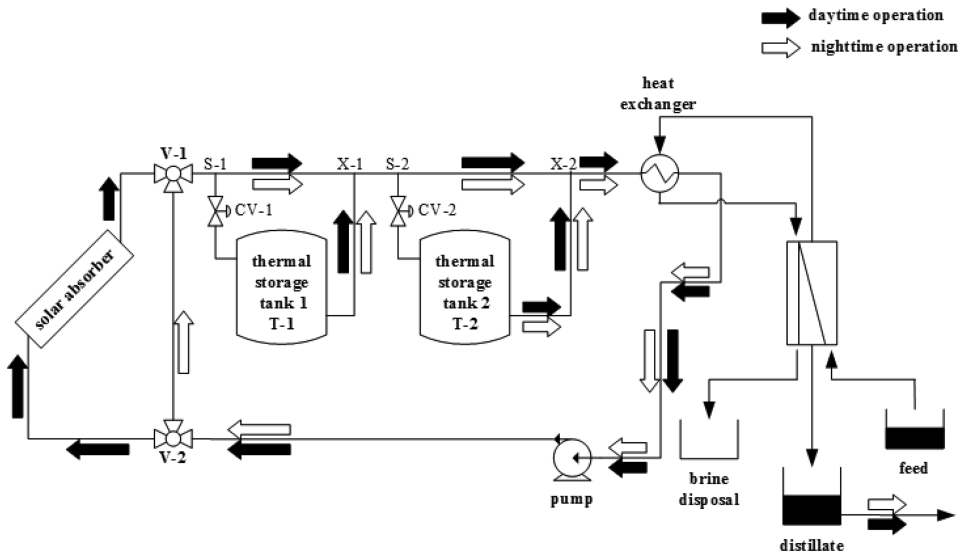


**Figure 12.** Structure 3 of SMDDS system.

As mentioned previously, the solar absorber should be sized according to the AGMD capacity. To facilitate proper evaluation and decision, the following asymptotic energy utilization ratio between these two units should be first defined:

$$\phi_{\text{util}} = \frac{\text{maximum supply rate of solar energy}}{\text{maximum consumption rate of thermal energy}} = \frac{A_{\text{SA}} I^{\max}}{m_{\text{MD}}^{\max} C_p (T_{\text{CL}_{\text{out}}}^{\text{HXmax}} - T_{\text{CL}_{\text{in}}}^{\text{HXmin}})} \quad (43)$$

where all symbols used in this equation can be found in Appendix I and, also, it is assumed that $T_{\text{CL}_{\text{out}}}^{\text{HX max}} = 90\ ^\circ\text{C}$ and $T_{\text{CL}_{\text{in}}}^{\text{HX min}} = 25\ ^\circ\text{C}$. From Figure 14, it can be observed that $I^{\max} = 1320\ \text{W/m}^2$. On the basis of eq A11 in Appendix I, one could deduce that $m_{\text{f,MD}}^{\max} = 1.1 m_{\text{f,MD}}^{N} = 1237.5$ kg/h. It should be noted that $\phi_{\text{util}}$ can be used as a convenient (but rough) design specification. The energy collected by the solar absorber could be fully utilized right away by the AGMD module if $\phi_{\text{util}} \leq 1$, while there should be a need to store the excess heat if otherwise.

The proposed mathematical programming models and their solution strategies have been utilized to facilitate quantitative flexibility analyses so as to provide the designers with the capabilities to (1) determine the performance measures of any system design in relation to the expected operational requirements, (2) identify the bottleneck conditions which limit the flexibility in a design, and (3) compare alternatives on an objective basis. A systematic approach is followed in this work to size the solar absorber on the basis of eq 43 and a given AGMD module size. By adopting the aforementioned thermal storage tank(s) and distillate tank, structures 1−4 can be analyzed for different utilization ratios. The resulting *dynamic* flexibility indices are presented in Table 1, while the *temporal* flexibility index and active constraint(s) in each scenario can also be found in the footnotes.

Let us first consider the dynamic flexibility indices:



DOI: 10.1021/acs.iecr.5b03593
*Ind. Eng. Chem. Res.* 2016, 55, 670−682

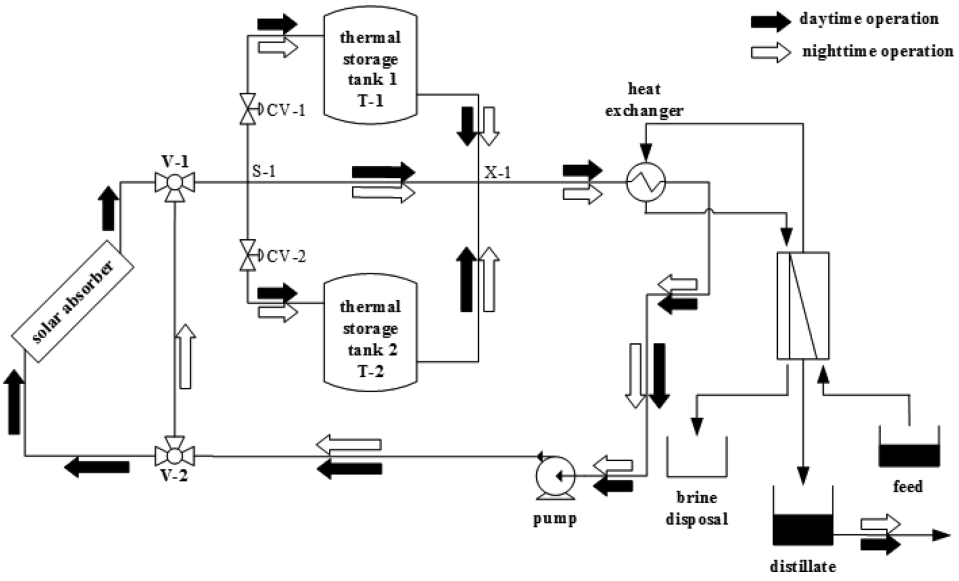


**Figure 13.** Structure 4 of SMDDS system.

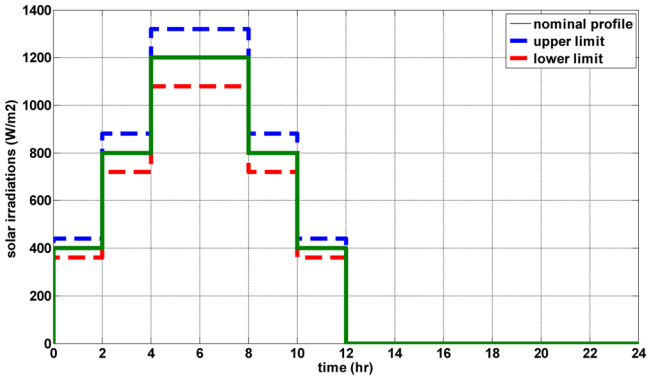


**Figure 14.** Solar irradiation rate.

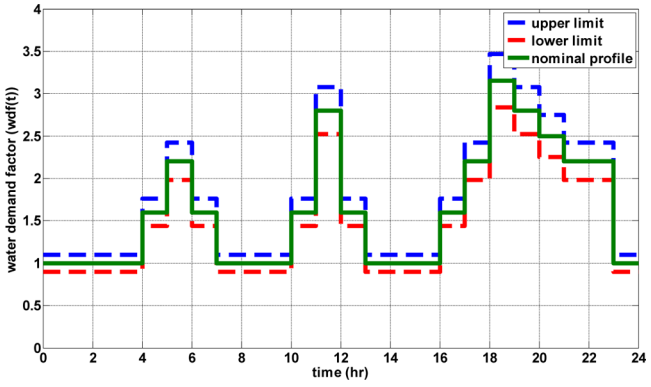


**Figure 15.** Water demand factor.

- It was observed from the optimization results of Case 1 and Case 2 that, when $\phi_{util} < 1$, all four structures yield the same flexibility index. This is because of the fact that, since the absorbed solar energy is consumed almost immediately and completely in these two cases, there is no need for the thermal storage tanks, i.e., $r_{ST,1}(t) = r_{ST,2}(t) = 0$, and thus all configurations are basically identical. Therefore, it is meaningless to list the index values repeatedly in Case 1 and Case 2.

**Table 1. Dynamic Flexibility Indices ($FI_d$) of Four Different SMDDS Structures**[a]

| | case 1 | case 2 | case 3 | case 4 | case 5 |
|---|---|---|---|---|---|
| structure | $\phi_{util} = 0.75$ | $\phi_{util} = 0.86$ | $\phi_{util} = 1.00$ | $\phi_{util} = 1.12$ | $\phi_{util} = 1.30$ |
| 1 | 0.415[b,e] | 1.0[b,f] | 1.077[c,f] | 0[c,h] | *i* |
| 2 | *s* | *s* | 1.46[b,f] | 1.64[c,f] | 0.59[c,d,g] |
| 3 | *s* | *s* | 1.48[b,f] | 1.95[b,f] | 1.244[c,d,f] |
| 4 | *s* | *s* | 1.48[b,f] | 1.95[b,f] | 1.244[c,d,f] |

[a]Notation: *i*, infeasible; *s*, superfluous scenario. [b]$h_{DT} = h_{DT,low}$. [c]$T_{SAout} = T_{SA_{out}}^{max}$. [d]$h_{DT} = h_{DT,low}$. [e]$FI_t = 0.72$. [f]$FI_t = 1.728$. [g]$FI_t = 0.86$. [h]$FI_t = 0.0$.

- Under the condition that $\phi_{util} \geq 1$ (i.e., cases 3−5), a few more conclusions can be drawn from the corresponding results:
  - A larger solar absorber tends to make structure 1 less flexible. In extreme conditions, the system may even approach zero flexibility (case 4) or infeasibility (case 5).
  - Although structures 2−4 are always more operable than structure 1, the dynamic flexibility index of each configuration reaches a maximum at $\phi_{util} = 1.12$ in case 4 and then drops to a lower value if the absorber size is further increased (see case 5).
  - Structures 3 and 4 are equally flexible, while they usually outperform structure 2.

In addition, one can also conclude from the corresponding temporal flexibility indices that

- The upper limit of $FI_t$, that is, 1.728, is reached as long as $FI_d \geq 1$. This is primarily due to the fact that, while an adjustable parameter range is adopted for computing $FI_d$ with eq 12, a fixed one is used for $FI_t$ according to eqs 5 and 14.
- $FI_d < FI_t$ if $0 < FI_d < 1$. This is in a sense caused by the relaxed criterion suggested in eqs 8 and 9.

Thus, although $FI_t$ is probably not useful for flexibility analysis when $FI_d \geq 1$, it may be adopted to identify less-expensive revamp designs when $FI_d < 1$. For example, let us consider structure 2 in case 5 (in which $FI_d = 0.59$ and $FI_t = 0.86$). Two alternative revamp options, i.e., enlarging the thermal storage



DOI: 10.1021/acs.iecr.5b03593
Ind. Eng. Chem. Res. 2016, 55, 670−682

tank(s) or enlarging the distillate tank, may be adopted to attain a "desired" flexibility level:

- The inventory of operating fluid must be increased from 10 000 to 15 000 kg if the design target is $FI_d = 1$, while only 11 000 kg is needed to realize $FI_t = 1$.
- The volume of distillate tank should be raised from 0.7490 $m^3$ to 0.8225 $m^3$ to achieve the former target, while only 0.7630 $m^3$ is called for to hit the latter goal.

## 7. CONCLUSIONS

In this study, the conventional vertex method has been modified to calculate the dynamic and temporal flexibility indices efficiently. Extensive case studies have also been carried out to confirm the effectiveness of the proposed algorithms. One can also see that, depending upon the availability of historical data and the intrinsic nature of uncertainty in the particular application, either $FI_d$ or $FI_t$ (or both) can be used to represent the operational flexibility of an unsteady process. Furthermore, a generic design procedure can be summarized accordingly as follows:

For any given design, the dynamic index should be computed first. If $FI_d \geq 1$, then of course no changes are needed. If otherwise, then the temporal index should also be determined according to the proposed mathematical program. The proper revamp measures (i.e., those for achieving $FI_d = 1$ or $FI_t = 1$) can be identified on the basis of the appropriateness of uncertainty characterization in the corresponding model and also their economic implications.

## APPENDIX I

The essential SMDDS units, that is, the solar absorber, the thermal storage tank, the counter-flow shell-and-tube heat exchanger, the AGMD modules, and the distillate tank, are interconnected in a typical system to form two separate processing routes for seawater desalination and solar energy conversion, respectively. For implementation convenience, the unit models given in Chang et al.[28] have been simplified and outlined below:[24]

### 1. Solar Absorber (SA)

The solar energy is converted to heat in this unit. The following basic assumptions are adopted: (i) the fluid velocities in all absorber tubes are the same; (ii) the fluid temperature should be kept below 100 °C; (iii) there is no water loss; (iv) heat loss is negligible. The corresponding transient energy balance and temperature constraint can be written as

$$\frac{dT_{SA_{out}}}{dt} = -\frac{m_{SA}}{M_{SA}}(T_{SA_{out}} - T_{SA_{in}}) + \frac{A_{SA}I(t)}{M_{SA}C_p} \tag{A1}$$

$$T_{SA_{out}} \leq T^{max}_{SA_{out}} \tag{A2}$$

where, $T_{SA_{in}}$ and $T_{SA_{out}}$ denote the temperatures (°C) of operating fluid at the inlet and outlet of the solar absorber respectively; $T^{max}_{SA_{out}}$ is the maximum allowable outlet temperature (100 °C) of the working fluid; $M_{SA}$ denotes the total mass of operating fluid in the solar absorber (kg); $m_{SA}$ denotes the mass flow rate of operating fluid in solar absorber (kg/h); $A_{SA}$ is the exposed area of solar absorber ($m^2$); $C_p$ is the heat capacity of operating fluid (J/(kg °C)); $I(t)$ is the solar irradiation rate per unit area (W/$m^2$) at time $t$. It should also be noted that the solar absorber is operable only in the daytime, that is,

$$m_{SA} = \begin{cases} m_{STL} & \text{if } I(t) > 0 \text{ (daytime)} \\ 0 & \text{if } I(t) = 0 \text{ (nighttime)} \end{cases} \tag{A3}$$

where $m_{STL}$ is the total mass flow rate (kg/h) of operating fluid which is driven by pump in the thermal loop.

### 2. Thermal Storage Tank (ST)

Based on the assumption that (i) the fluid within the thermal storage tank is well mixed, (ii) the inlet and outlet flow rates are identical, and (iii) the heat capacity of operating fluid is independent of temperature, the energy balance around thermal storage tank can be expressed as

$$M_{ST,i}\frac{dT_{ST_{out},i}}{dt} = m_{ST,i}(T_{ST_{in},i} - T_{ST_{out},i}) \tag{A4}$$

$$m_{ST,i} = r_{ST,i}m_{STL} \tag{A5}$$

where, subscript $i$ is a tank label ($i = 1, 2$); $T_{ST_{in},i}$ and $T_{ST_{out},i}$ denote the fluid temperatures (°C) at the inlet and outlet of tank $i$ ,respectively; $M_{ST,i}$ represents the total mass of operating fluid in tank $i$ (kg); $m_{STL}$ is the total mass flow rate driven by the pump in the thermal loop (kg/h); $m_{ST,i}$ is the throughput of tank (kg/h). The flow ratios defined by eq A5, that is, $r_{ST,1}$ and $r_{ST,2}$, are treated as control variables which can be adjusted with valves CV-1 (see Figures 11−13) and CV-2 (see Figures 12 and 13). Clearly these ratios vary between 0 and 1, that is,

$$0 \leq r_{ST,i}(t) \leq 1 \tag{A6}$$

Also, the speed of valve movement in practice cannot be unbounded; that is,

$$\left|\frac{dr_{ST,i}}{dt}\right| \leq rr_i^{max} \tag{A7}$$

where, $rr_i^{max}$ is a given constant.

### 3. Heat Exchanger (HX)

The hot fluid used in the counter-flow heat exchanger comes from the thermal storage tank and/or solar absorber, while the cold fluid is the sea water. The heat exchanger is assumed to be always in steady-state and there is no heat loss. Thus, the unit model of heat exchanger can be written as

$$m_{MD}(T^{HX}_{CL_{out}} - T^{HX}_{CL_{in}}) = m^{HX}_{HL}(T^{HX}_{HL_{in}} - T^{HX}_{HL_{out}}) \tag{A8}$$

where, $m^{HX}_{HL}$ is the mass flow rate of hot fluid (kg/h); $T^{HX}_{HL_{in}}$ and $T^{HX}_{HL_{out}}$, respectively, denote the inlet and outlet temperatures of hot fluid (°C); $m_{MD}$ is the mass flow rate of sea water in membrane distillation loop (kg/h); $T^{HX}_{CL_{in}}$ and $T^{HX}_{CL_{out}}$ respectively denote the inlet and outlet temperatures of the cold fluid (°C). Note that the mass flow rate of hot fluid is essentially the same as that in the thermal loop in any structure:

$$m^{HX}_{HL} = m_{STL} \tag{A9}$$

### 4. Air Gap Membrane Distillation Module (AGMD)

A simplified model is adopted in this study for characterizing the AGMD unit. Although the mass flux through AGMD membrane is driven primarily by the vapor pressure differential, it is assumed that the mass flux of distillate across the membrane is a function of the rate of energy input. Specifically, this flux in a standard module can be expressed as



DOI: 10.1021/acs.iecr.5b03593
Ind. Eng. Chem. Res. 2016, 55, 670−682

$$N_{mem} \cong \frac{m_{MD} C_p (T^{HX}_{CL_{out}} - T^{HX}_{CL_{in}})}{STEC \cdot A_{MD} \cdot n_{AGMD}} \quad (A10)$$

where, $N_{mem}$ denotes the distillate flux (kg/(m$^2$ h)); $A_{MD}$ is the fixed membrane area of a standard AGMD module (i.e., 10 m$^2$); $n_{AGMD}$ is the total number of standard modules; STEC is the specific thermal energy consumption constant (kJ/kg), which can be considered as the ratio between energy supplied by the heat exchanger and mass of the distillate produced (Banat et al., 2007; Burgess and Lovegrove, 2005).

Since eq A10 is empirical, it should be only valid within a finite range of the sea water flow rate. Consequently, $m_{MD}$ is treated in this work also as a control variable which is allowed to vary ±10% from its nominal value.

$$0.9 \times m^N_{MD} \le m_{MD} \le 1.1 \times m^N_{MD} (= m^{max}_{MD}) \quad (A11)$$

Finally, note that the sea water entering the AGMD module should not be allowed to exceed a specified upper bound so as to avoid damaging the membrane:

$$T^{HX}_{CL_{out}} \le T^{HXmax}_{CL_{out}} \quad (A12)$$

where, $T^{HX\ max}_{CL_{out}}$ is the upper bound of cold stream temperature at the outlet of heat exchanger (90 °C).

### 5. Distillate Tank (DT)

The distillate tank is acting as the buffer for the fluctuating water demand. Its model can be expressed as

$$\rho A_{DT} \frac{dh_{DT}}{dt} = m_{DT_{in}} - m_{DT_{out}} \quad (A13)$$

where $\rho$ is the distillate density (kg/m$^3$); $A_{DT}$ is the cross-sectional area of distillate tank (m$^2$); $h_{DT}$ is the height of liquid in distillate tank (m); $m_{DT_{in}}$ and $m_{DT_{out}}$ denote the inlet and outlet flow rates respectively (kg/h). Note that the inlet flow is produced by the AGMD unit:

$$m_{DT_{in}} = n_{AGMD} N_{mem} A_{MD} \quad (A14)$$

Finally, the liquid height in the distillate tank should be maintained within a specified range:

$$h_{DT,low} \le h_{DT} \le h_{DT,high} \quad (A15)$$

where, $h_{DT,low}$ and $h_{DT,high}$ respectively denote the given lower and upper bounds (m).

### 6. 3-Way Valves (V-1 and V-2)

*V-1.* In structures 2−4, the mass and energy balances around V-1 can be written as

$$m_{S-1} = \begin{cases} m_{SA} & \text{if } I(t) > 0 \\ m_{STL} & \text{if } I(t) = 0 \end{cases} \quad (A16)$$

$$T_{S-1} = \begin{cases} T_{SAout} & \text{if } I(t) > 0 \\ T^{HX}_{HLout} & \text{if } I(t) = 0 \end{cases} \quad (A17)$$

where, $m_{S-1}$ and $T_{S-1}$ respectively denote the mass flow rate (kg/h) and temperature (°C) of the stream leaving V-1.

*V-2.* On the other hand, the mass and energy balances around V-2 in structures 2−4 should be expressed as

$$m_{STL} = \begin{cases} m_{SA} & \text{if } I(t) > 0 \\ m_{S-1} & \text{if } I(t) = 0 \end{cases} \quad (A18)$$

$$T^{HX}_{HLout} = \begin{cases} T_{SAin} & \text{if } I(t) > 0 \\ T_{S-1} & \text{if } I(t) = 0 \end{cases} \quad (A19)$$

### 7. Split Points (S-1 and S-2)

*S-1.* In structures 2 and 3, the operating fluid leaving 3-way valve V-1 is split into two streams via S-1. One of them is directed to the thermal storage tank, that is, T (structure 2) or T-1 (structure 3), while the other bypasses the tank and joins its output at the mixing point X-1. The corresponding mass and energy balances can be written as

$$m_{S-1} = m_{ST,1} + m_{X-1} \quad (A20)$$

$$T_{S-1} = T_{STin,1} = T_{X-1} \quad (A21)$$

where, $m_{X-1}$ represents the mass flow rate of the bypass stream from S-1 to X-1 (kg/h) and $T_{X-1}$ is the corresponding temperature (°C).

On the other hand, note that in structure 4 the operating fluid leaving 3-way valve V-1 is split into three streams via S-1. Two of them are directed toward T-1 and T-2, respectively, while the remaining one bypasses both tanks and joins the outlet streams of these tanks at the mixing point X-1. The corresponding mass and energy balances should be

$$m_{S-1} = m_{ST,1} + m_{ST,2} + m_{X-1} \quad (A22)$$

$$T_{S-1} = T_{STin,1} = T_{STin,2} = T_{X-1} \quad (A23)$$

From eq A22, one can also deduce the following inequality constraint

$$0 \le r_{ST,1} + r_{ST,2} \le 1 \quad (A24)$$

*S-2.* The second split point is only present in series structure (see Figure 12). Note that the stream leaving X-1 is split into two via S-2. One flows into tank T-2, while the other bypasses the tank and joins its output at the mixing point X-2. The mass and energy balances around S-2 can be expressed as follows:

$$m_{STL} = m_{ST,2} + m_{X-2} \quad (A25)$$

$$T_{S-2} = T_{STin,2} = T_{X-2} \quad (A26)$$

where, $m_{X-2}$ represents the mass flow rate of the bypass stream from S-2 to X-2 (kg/h) and $T_{X-2}$ is the corresponding temperature (°C).

### 8. Merge Points (X-1 and X-2)

*X-1.* In structure 2, the energy balance around X-1 can be formulated as

$$T^{HX}_{HL_{in}} = (1 - r_{ST,1}) T_{X-1} + r_{ST,1} T_{ST_{out},1} \quad (A27)$$

In structure 3, the corresponding energy balance equation is

$$T_{S-2} = (1 - r_{ST,1}) T_{X-1} + r_{ST,1} T_{ST_{out},1} \quad (A28)$$

In structure 4, the corresponding energy balance equation is

$$T^{HX}_{HL_{in}} = (1 - r_{ST,1} - r_{ST,2}) T_{X-1} + r_{ST,1} T_{ST_{out},1} + r_{ST,2} T_{ST_{out},2} \quad (A29)$$

*X-2.* Mixing point X-2 is used only in structure 3, and the corresponding energy balance can be written as

$$T^{HX}_{HL_{in}} = (1 - r_{ST,2}) T_{X-2} + r_{ST,2} T_{ST_{out},2} \quad (A30)$$



DOI: 10.1021/acs.iecr.5b03593
Ind. Eng. Chem. Res. 2016, 55, 670−682

**Table AII**

| symbol | definition | value | type |
|---|---|---|---|
| $A_{SA}$ | exposed area of solar absorber | | d |
| $A_{MD}$ | membrane area of AGMD module | 40 $m^2$ | d |
| $A_{DT}$ | cross-sectional area of distillate tank | 0.35 $m^2$ | d |
| $T_{SA_{out}}^{max}$ | maximum outlet temperature of solar absorber | 100 °C | d |
| $T_{CL_{out}}^{HX\ max}$ | maximum cold stream temperature at outlet of heat exchanger | 90 °C | d |
| $T_{CL_{in}}^{HX}$ | cold stream temperature at inlet of heat exchanger | 25 °C | d |
| $M_{SA}$ | total mass of operating fluid in solar absorber | | d |
| $M_{ST,i}$ | total mass of operating fluid in thermal storage tank $i$ | 10000 kg | d |
| $m_{STL}$ | mass flow rate in thermal loop | 36000 kg/h | d |
| $m_{MD}^{N}$ | mass flow rate in membrane distillation loop | 4500 kg/h | d |
| $m_{MD}^{max}$ | maximum mass flow rate in membrane distillation loop | 4950 kg/h | d |
| $L_{SA}$ | length of absorber tube | | d |
| $C_p$ | heat capacity of operating fluid | 4200 J/(kg °C) | d |
| $\rho$ | distillate density | 1000 $kg/m^3$ | d |
| $n_{AGMD}$ | total number of standard AGMD modules | 4 | d |
| STEC | specific thermal energy consumption constant | 14000 kJ/kg | d |
| $h_{DT,low}$ | lower bound of liquid height in distillate tank | 0 m | d |
| $h_{DT,high}$ | upper bound of liquid height in distillate tank | 2.14 m | d |
| $I^{max}$ | maximum solar irradiation rate per unit area | 1320 $W/m^2$ | d |
| $rr_i^{max}$ | maximum variation rate of flow ratio $i$ | 0.01 | d |
| $\phi_{util}$ | energy utilization ratio | | d |
| $T_{SA_{out}}$ | inlet temperature of solar absorber | | x |
| $T_{SA_{in}}$ | outlet temperature of solar absorber | | x |
| $T_{ST_{out},i}$ | outlet temperature of thermal storage tank $i$ | | x |
| $T_{ST_{in},i}$ | inlet temperature of thermal storage tank $i$ | | x |
| $T_{S\text{-}1}$ | temperature at split point S-1 | | x |
| $T_{S\text{-}2}$ | temperature at split point S-2 | | x |
| $T_{X\text{-}1}$ | temperature at merge point X-1 | | x |
| $T_{X\text{-}2}$ | temperature at merge point X-2 | | x |
| $T_{HL_{out}}^{HX}$ | hot stream temperature at outlet of heat exchanger | | x |
| $T_{HL_{in}}^{HX}$ | hot stream temperature at inlet of heat exchanger | | x |
| $T_{CL_{out}}^{HX}$ | cold stream temperature at outlet of heat exchanger | | x |
| $m_{SA}$ | mass flow rate of operating fluid in solar absorber | | x |
| $m_{ST,i}$ | throughput of thermal storage tank $i$ | | x |
| $m_{HL}^{HX}$ | mass flow rate of hot stream in heat exchanger | | x |
| $m_{DT_{in}}$ | mass flow rate at inlet of distillate tank | | x |
| $m_{S\text{-}1}$ | mass flow rate of the stream entering split point S-1 | | x |
| $m_{X\text{-}1}$ | mass flow rate of the bypass stream from S-1 to X-1 | | x |
| $m_{X\text{-}2}$ | mass flow rate of the bypass stream from S-2 to X-2 | | x |
| $N_{mem}$ | distillate flux through AGMD membrane | | x |
| $h_{DT}$ | liquid height in distillate tank | | x |
| $m_{MD}$ | mass flow rate in membrane distillation loop | | z |
| $r_{ST,i}$ | flow ratio of split stream directed toward thermal storage tank $i$ | | z |
| $I$ | solar irradiation rate per unit area | | $\theta$ |
| $m_{DT_{out}}$ | outlet flow rate of distillate tank | | $\theta$ |

## APPENDIX II: NOMENCLATURE FOR THE SMDDS MODEL

All model parameters and variables used in the case studies are listed in Table AII.

## AUTHOR INFORMATION


### Corresponding Author

*Email: ctchang@mail.ncku.edu.tw.


### Notes

The authors declare no competing financial interest.

## REFERENCES


(1) Malcom, A.; Polan, J.; Zhang, L.; Ogunnaike, B. A.; Linninger, A. A. Integrating system design and control using dynamic flexibility analysis. *AIChE J.* **2007**, *53*, 2048.

(2) Lima, F. V.; Georgakis, C. Design of output constraints for model-based non-square controllers using interval operability. *J. Process Control* **2008**, *18*, 610.

(3) Lima, F. V.; Georgakis, C.; Smith, J. F.; Schnelle, P. D.; Vinson, D. R. Operability-based determination of feasible control constraints for several high-dimensional nonsquare industrial processes. *AIChE J.* **2009**, *55*, 1249.

(4) Lima, F. V.; Jia, Z.; Ierapetritou, M.; Georgakis, C. Similarities and differences between the concepts of operability and flexibility: The steady-state case. *AIChE J.* **2010**, *56*, 702.

(5) Swaney, R. E.; Grossmann, I. E. An index for operational flexibility in chemical process design. Part I: formulation and theory. *AIChE J.* **1985**, *31*, 621.

(6) Swaney, R. E.; Grossmann, I. E. An index for operational flexibility in chemical process design. Part II: computational algorithms. *AIChE J.* **1985**, *31*, 631.

(7) Grossmann, I. E.; Halemane, K. P. Decomposition strategy for designing flexible chemical plants. *AIChE J.* **1982**, *28*, 686.

(8) Halemane, K. P.; Grossmann, I. E. Optimal process design under uncertainty. *AIChE J.* **1983**, *29*, 425.

(9) Grossmann, I. E.; Floudas, C. A. Active constraint strategy for flexibility analysis in chemical process. *Comput. Chem. Eng.* **1987**, *11*, 675.

(10) Varvarezos, D. K.; Grossmann, I. E.; Biegler, L. T. A sensitivity-based approach for flexibility analysis and design of linear process systems. *Comput. Chem. Eng.* **1995**, *19*, 1301.

(11) Bansal, V.; Perkins, J. D.; Pistikopoulos, E. N. Flexibility analysis and design of linear systems by parametric programming. *AIChE J.* **2000**, *46*, 335.

(12) Floudas, C. A.; Gunus, Z. H.; Ierapetritou, M. G. Global optimization in design under uncertainty: feasibility test and flexibility index problems. *Ind. Eng. Chem. Res.* **2001**, *40*, 4267.

(13) Ostrovski, G. M.; Achenie, L. E. K.; Wang, Y. P.; Volin, Y. M. A new algorithm for computing process flexibility. *Ind. Eng. Chem. Res.* **2001**, *39*, 2368.

(14) Ostrovski, G. M.; Volin, Y. M. Flexibility analysis of chemical process: Selected global optimization sub-problems. *Optim. Eng.* **2002**, *3*, 31.




DOI: 10.1021/acs.iecr.5b03593
*Ind. Eng. Chem. Res.* 2016, 55, 670−682

(15) Bansal, V.; Perkins, J. D.; Pistikopoulos, E. N. Flexibility analysis and design using a parametric programming framework. *AIChE J.* **2002**, *48*, 2851.
(16) Volin, Y. M.; Ostrovski, G. M. Flexibility analysis of complex technical systems under uncertainty. *Autom. Remote Control* **2002**, *63*, 1123.
(17) Chang, C. T.; Li, B. H.; Liou, C. W. Development of a generalized mixed integer nonlinear programming model for assessing and improving the operational flexibility of water network designs. *Ind. Eng. Chem. Res.* **2009**, *48*, 3496.
(18) Riyanto, E.; Chang, C. T. A heuristic revamp strategy to improve operational flexibility of water networks based on active constraints. *Chem. Eng. Sci.* **2010**, *65*, 2758.
(19) Jiang, H.; Chen, B.; Wang, H.; Qiu, T.; Zhao, J. Novel method for considering process flexibility and stability simultaneously. *Ind. Eng. Chem. Res.* **2014**, *53*, 14765.
(20) Dimitriadis, V. D.; Pistikopoulos, E. N. Flexibility analysis of dynamic system. *Ind. Eng. Chem. Res.* **1995**, *34*, 4451.
(21) Dimitriadis, V. D.; Shah, N.; Pantelides, C. C. Modeling and safety verification of discrete/continuous processing systems. *AIChE J.* **1997**, *43*, 1041.
(22) Zhou, H.; Li, X. X.; Qian, Y.; Chen, Y.; Kraslawski, A. Optimizing the initial conditions to improve the dynamic flexibility of batch processes. *Ind. Eng. Chem. Res.* **2009**, *48*, 6321.
(23) Adi, V. S. K.; Chang, C. T. A mathematical programming formulation for temporal flexibility analysis. *Comput. Chem. Eng.* **2013**, *57*, 151.
(24) Adi, V. S. K.; Chang, C. T. SMDDS design based on temporal flexibility analysis. *Desalination* **2013**, *320*, 96.
(25) Adi, V. S. K.; Chang, C. T. Development of flexible designs for PVFC hybrid power systems. *Renewable Energy* **2015**, *74*, 176.
(26) Biegler, L. T., Grossmann, E. I.; Westerberg, A. W. *Systematic Methods of Chemical Process Design*; Prentice Hall: Upper Saddle River, NJ, 1997; pp 701−702.
(27) Ben Bacha, H.; Dammak, T.; Ben Abdalah, A. A.; Maalej, A. Y.; Ben Dhia, H. Desalination unit coupled with solar collectors and storage tank: modeling and simulation. *Desalination* **2007**, *206*, 341.
(28) Chang, H.; Wang, G. B.; Chen, Y. H.; Li, C. C.; Chang, C. L. Modeling and optimization of a solar driven membrane distillation desalination system. *Renewable Energy* **2010**, *35*, 2714.
(29) Chang, H.; Lyu, S. G.; Tsai, C. M.; Chen, Y. H.; Cheng, T. W.; Chou, Y. H. Experimental and simulation study of a solar thermal driven membrane distillation desalination process. *Desalination* **2012**, *286*, 400.
(30) Banat, F.; Jwaied, N.; Rommel, M.; Koschikowski, J.; Wieghaus, M. Performance evaluation of the "large SMADES" autonomous desalination solar-driven membrane distillation plant in Aqaba, Jordan. *Desalination* **2007**, *217*, 17.


DOI: 10.1021/acs.iecr.5b03593
*Ind. Eng. Chem. Res.* 2016, 55, 670−682